Screening Earth Analog Exoplanets on the Basis of a Predicted Nitrogen over Phosphorus Ratio

Hervé Toulhoat

The Astrophysical Journal, 958:124 (15pp), 2023 December 1 https://doi.org/10.3847/1538-4357/acfc4e

Screening Earth Analog Exoplanets on the Basis of a Predicted Nitrogen over Phosphorus Ratio

Hervé Toulhoat
Laboratoire de Réactivité de Surface, Sorbonne Université; Paris, F-75252 Cedex 05, France; herve.toulhoat@orange.fr
Received 2023 June 21; revised 2023 August 23; accepted 2023 September 15; published 2023 November 17

Abstract

Since the first discovery in 1995, data for over 5300 exoplanets have been documented in the NASA archive, revealing a vast diversity. Identifying life-enabling analogs of the Earth among this rapidly expanding catalog is of major interest. The stability of liquid water at the planetary surface defining the concept of the habitable zone (HZ) around the host star, may be necessary for the emergence of life as we know it but not sufficient. The practically constant atomic ratio nitrogen:phosphorous = 16:1 in oceanic surface layers of our planet Earth was discovered by Redfield in 1934. It corresponds to phytoplanktonic biomass in suspension and appears optimal to fertilize phytoplankton development and therefore the food pyramid of marine life. Loladze and Elser have shown that it corresponds to a homeostatic protein:RNA ratio and is therefore "rooted in the stoichiometry of the foundational structures of life." I show that according to the recent theory of the chemical differentiation of planets, this optimal ratio is also an intrinsic chemical property of our planet Earth uniquely determined in the solar system by its average orbital radius. On that basis, I propose a criterion of fertility within the HZ of a stellar system, which when applied to screen the public database allows us to sort out an extended list of up to 74 Earth analogs. The latter and its future extensions could provide priority targets for focused detection techniques.

Unified Astronomy Thesaurus concepts: Astrobiology (74); Biosignatures (2018); Astrochemistry (75); Chemical abundances (224)

1. Introduction

The practically constant ratio of nitrates to phosphates in oceanic surface layers of our planet Earth was discovered by Redfield (1934, 1936, 1958). It corresponds to phytoplanktonic biomass in suspension, which is also characterized by an average atomic ratio close to N:P = 16:1. This ratio appears optimal to fertilize phytoplankton development and therefore the food pyramid of marine life. Whether this ratio of nutrients was the cause or is a consequence, of the emergence of photosynthetic organisms has been debated (Falkowski & Davis 2004; Bertrand & Legendre 2021) and remains an open question. It has been shown that it corresponds to a homeostatic protein:RNA ratio and is therefore "rooted in the stoichiometry of the foundational structures of life" (Loladze & Elser 2011). I propose here that this optimal ratio is also an intrinsic chemical property of our planet Earth, and that a criterion based on a critical distance to the host star should allow for a refined screening of exoplanets databases for Earth analogs.

2. Theoretical Background

Recently we proposed a novel scenario for the early chemical differentiation of gaseous protoplanetary disks and therefore later condensed planets (Toulhoat & Zgonnik 2022): at a radial distance d from the energetic photons emitting protostar, ionized atoms are stabilized in orbit by Lorenz forces. The local mass fraction X(A, d) of ionized element A at distance d is shown to obey the following law:

$$\frac{\mathrm{X}(A,d)\,/\,\mathrm{X}(\mathrm{Si},d)}{\mathrm{X_{SS}}(A)\,/\,\mathrm{X_{SS}}(\mathrm{Si})} = exp\left[\frac{(-\mathrm{IP(A)}+\mathrm{IP(Si)})}{k_B T_G(d)}\pi\left(\frac{R_{\mathrm{PS}}}{d}\right)^2\right], \quad (1)$$

where $\mathrm{X_{SS}}(A)$ is the initial mass fraction in the nebula fixed by nucleosynthesis, IP(A) is the first ionization potential of element A, k_B is the Boltzmann constant, R_{PS} is the protostar radius, and $T_G(d)$ is the local temperature of the partially ionized gas. Terms $\frac{\mathrm{X}(A,d)\,/\,\mathrm{X}(\mathrm{Si},d)}{\mathrm{X_{SS}}(A)\,/\,\mathrm{X_{SS}}(\mathrm{Si})}$ are referred to as "differentiation factors." In what follows, for convenience, we refer to this scenario as the "photophysical model."

For our solar system, the average compositions of planetary surface rocks sampled thanks to past space missions to Mercury, Venus, the Moon, and Mars, compared to those of the Earth and meteorites show that:

for $d < 1$ au:

$$T_G(d) = T_{\mathrm{CB}}\frac{1}{d^3}, \quad (2)$$

while for $d \geqslant 1$ au (that is beyond the Earth):

$$T_G(d) = T_{\mathrm{CB}}. \quad (3)$$

It follows that our home planet is in orbit at a very special position: a cusp point on the radial distribution profile of any element in the solar system.

Considering further radial distribution profiles of atomic ratio $\rho_{\mathrm{A/B}}$ of element A over B, one gets:

for $d < 1$ au:

$$\rho_{\mathrm{A/B}}(d) = P_{\mathrm{AB}}\exp\left[\frac{\delta_{\mathrm{AB}}\mathrm{IP}}{k_B T_{\mathrm{CB}}}\pi R_{\mathrm{PS}}^2 d\right], \quad (4)$$

and for $d \geqslant 1$ au:

$$\rho_{A/B}(d) = P_{AB} \exp\left[\frac{\delta_{AB}IP}{k_B T_{CB}} \pi \left(\frac{R_{PS}}{d}\right)^2\right], \quad (5)$$

with notations $P_{AB} = \frac{X_{SS}(A)\,/\,X_{SS}(Si)\,M_B}{X_{SS}(B)\,/\,X_{SS}(Si)\,M_A}$ and $\delta_{AB}IP = IP(B) - IP(A)$, where M_A is the atomic weight of element A. Terms $X_{SS}(A)/X_{SS}(Si)$ are the well-known relative abundances in the solar photosphere referred to the element Silicium. The protosolar radius was inferred from the differentiation factors of noble gases on Earth as $R_{PS} \cong 1.5R_S$, where R_S is the present-time solar radius (Toulhoat & Zgonnik 2022).

As shown in the Appendix, Section A.1, the cusp point at $d = 1$ au is a minimum for $\delta_{AB}IP < 0$ and a maximum for $\delta_{AB}IP > 0$.

3. Radial Distribution Profiles of Atomic Ratios across the Solar System

Table 1 displays numerical values allowing us to figure out the predicted profiles for the main elements involved in biomasses, C, H, O, N, and P.

Table 2 displays $\rho_{A/B}(1)$ for selected combinations and the main features of the corresponding radial profiles. The N/P profile across the solar system is shown in Figure 1.

The most striking result is $\rho_{N/P}(1) = 16.01$, identical within the error margin to the Redfield ratio: this means that according to our photophysical model, our planet Earth would have offered from the beginning precisely the ratio of essential nutrients necessary for the emergence and blooming of marine phytoplankton. This step in the evolution of life on Earth meant the onset of O_2-producing photosynthesis and further a basis for the food pyramid of marine life up to the present time.

Moreover, as shown in Figure 1, $\rho_{N/P}(d)$ increases rapidly for orbits closer to the Sun, or farther than the Earth, so that for Mercury, Venus, and Mars for instance, the availability of Phosphorus decreases with respect to Nitrogen. Too hot or too cold surface temperatures on these planets, and the apparent absence of liquid water, may be sufficient to explain their sterility. However, the imbalanced $\rho_{N/P}(d)$ could be another crucial detrimental factor to life-enhanced habitability as opposed to what prevailed for the Earth (i.e., an appropriate greenhouse effect and a protecting ozone layer).

Notice that $\rho_{A/B}(d)$ predicted for the protoplanetary disk holds in first approximation as averages for the bulk planets in orbit at distance d. For the Earth, chemical differentiation should generally further occur between the surface and bulk of planets due to various matter transfer processes. As underlined in our previous report (Toulhoat & Zgonnik 2022), measurements of the average elementary composition of the planet Earth are available only for superficial samples. The photophysical model predicts bulk values, and their comparison with surface values yields elemental partition coefficients between bulk and surface. The latter appear correlated with thermochemical properties, indicative of a progressive radial chemical differentiation of the Earth in response to an outward reactive flow of hydrogen driving the most electronegative elements (O and the halogens) to end up at the surface as acidic water, further neutralized into the oceans. In turn, the gradient of oxygen chemical potential thus established tends to drive the outward radial migration of elements according to their affinity for oxygen. The average atomic ratio N:P on the surface is 0.04, quite far from the predicted bulk N:P of 16, which coincides with the Redfield ratio. However, the latter is actually the molar ratio nitrates:phosphates (NO_3^-:PO_4^{3-}), the most oxidized species for nitrogen and phosphorus, and "hard anions" highly soluble in liquid water. Oceans are connected with the Earth's interior mostly through ridges at the junctions of oceanic floor tectonic plates, where deep vents deliver permanent hydrothermal fluids (HF). These fluids have been sampled and subjected to chemical analysis after numerous scientific expeditions in the past 40 years since the discovery of these deep-seafloor vents. The open-access MARHYS 2.0 database collects this information systematically for circa 3400 samples so far (Diehl & Bach 2020). Selecting HF samples, NO_3^- and PO_4^{3-} contents at the μmol kg^{-1} level yield an average N:P ratio of 16.6, in conformity with the Redfield ratio, which is otherwise very much documented in oceans seawater. CO_2 and N_2 contents, which at the mmol kg^{-1} level include the vast majority of C and N atoms in HF samples are available simultaneously for 113 samples. These data yield an average C:N ratio of 29.7, consistent with the model prediction of 30.1. Then, as the majority of O atoms the HF samples outside water itself are reported as conveyed by dissolved gases CO_2, SO_2, and the SO_4^{2-} anion, at on average 50.4, 38.2, and 13.1 mmol kg^{-1} levels, it is easy to compute an average C:O molar ratio of 2.3 also very consistent with the model prediction of 2.3. For the contents in other elements or species available in the database, such agreements between predicted and experimental ratios are generally not obtained, except for combinations of lanthanides, well documented simultaneously for up to 260 samples: average Cerium:X ratios, where X is another lanthanide (at the pmol kg^{-1} levels) appear well correlated with model predictions ($R^2 = 0.85$). Although the precise speciation of these elements is not reported, it is expected that their oxidation number in hydrothermal fluids is +3, generally the most stable for rare earths. As for noble gases, Only He, Ar, and Ne contents are reported simultaneously for at most circa 60 samples. Average molar ratios of these gases dissolved in hydrothermal fluids do not match the

Table 1
Properties of Elements Involved in Equations (1)–(5)

Element	$X_{SS}(A)/X_{SS}(Si)$(*)	M_A (g.mol^{-1})	IP(A) (eV)
C	3.027 10^0	12.011	11.256
H	1.035 10^3	1.008	13.595
O	8.05 10^0	15.999	13.614
N	0.9725 10^0	14.007	14.53
P	9.83 10^{-3}	30.974	10.484

Note. (*): Mass fraction referred to Si in the Sun photosphere (Lodders 2003).

Table 2
Main Features of Selected Radial Profiles of Elemental Ratios in the Solar System (Calculations Performed with $R_{PS} = 1.50\,R_S$, $R_S = 0.00465476$ au, $k_B = 8.61733\ 10^{-5}$ eV K^{-1}, and $T_{CB} = 2.75$ K)

A/B	$\rho_{\frac{A}{B}}(1)$	$\delta_{AB}IP$ (eV)	Nature of the Cusp
H/O	2066.26	0.019	Maximum
C/H	0.00111	2.339	Maximum
C/O	2.30	2.358	Maximum
C/N	30.12	3.274	Maximum
N/P	16.01	−4.046	Minimum

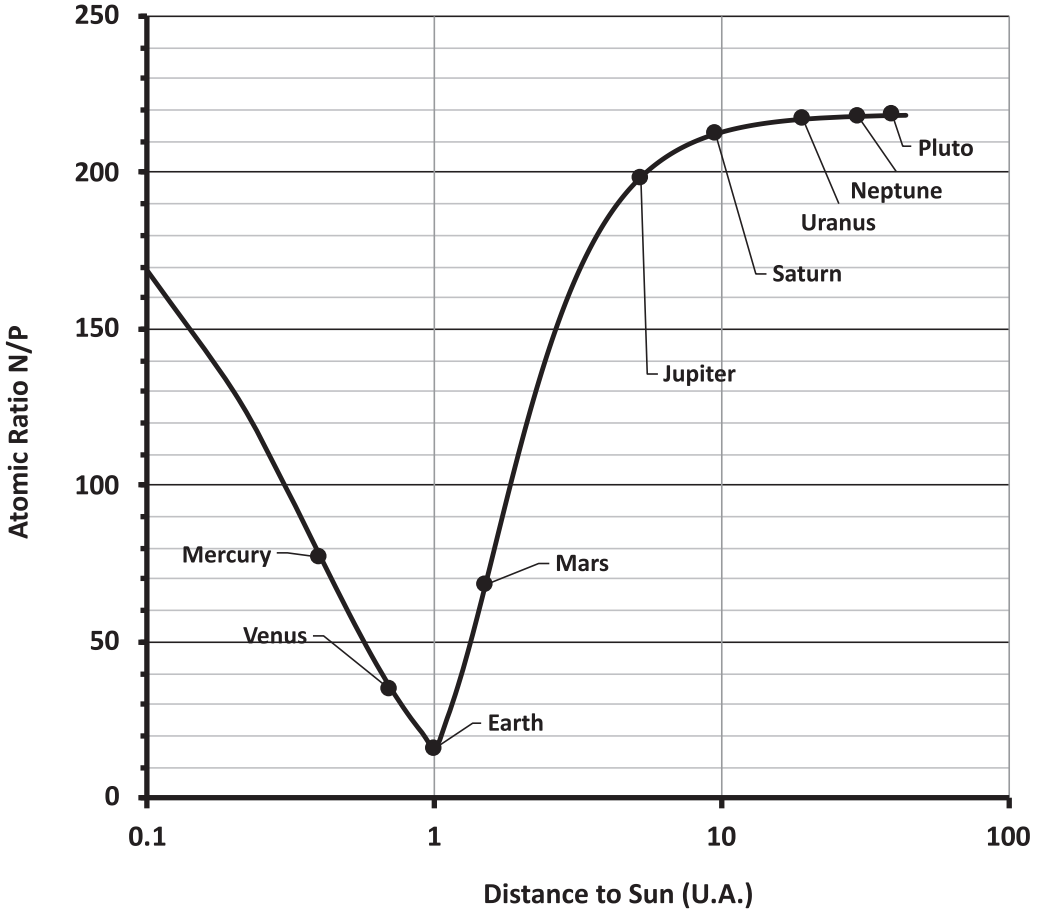

Figure 1. Atomic ratio N/P in the solar system as a function of the distance to the Sun, in au, as predicted by the "photophysical model." On Earth, this ratio is predicted to coincide with the Redfield ratio (N/P = 16) characterizing oceanic phytoplankton.

predictions, with Ar present on average at the 50 μmol kg^{-1} level, compared to 3 and 1 for Ne and He, respectively, while predictions are 0.013 for Ar:He, and 2.03 for Ar:Ne. Clearly, hydrothermal fluids from ocean floor vents are significantly enriched in Ar compared to the other noble gases, probably mostly radiogenic ^{40}Ar due to the decay of ^{40}K in the subsurface, not taken into account by the photophysical model. The Ne:He ratio of 3 in HF samples is not consistent with the prediction of 0.064 but rather with the ratio of 3.15 expected at the Earth's surface, which should reflect rather the relative Jeans escape flows of these lighter noble gases. A more extended discussion involving other couples of elements based on MARHYS data is certainly possible and scientifically interesting but beyond the scope of this first report. However, it is possible to conclude that on Earth, $\rho_{A/B}$ predicted by the photophysical model for the bulk planet is observed in oceans, not only as the Redfield ratio NO_3^-:PO_4^{3-}, but also as molar ratios of other fully oxidized species, still fed upwards from the Earth interior, through deep seafloor hydrothermal vents.

4. A New Screening Criterion for Fertilizable Exoplanets

Consider an exoplanet orbiting at a distance d_{Star} from its host star. As the photophysical model should hold for the chemical differentiation of any planetary system, a critical distance d^* to the host star analogous to the Earth–Sun distance should be found systematically. Equations (4), (5), and (A1)–(A3) should apply with lengths expressed in astronomic units scaled by $\frac{1}{d^*}$ (see the Appendix, Section A.3). The function $\rho_{N/P}(d_{Star}/d^* = 1)$ would then be a minimum at a cusp point. According to Equation (A1), its value should be exponentially inverse dependent on the squared rescaled protostar radius $\frac{R_{PS}}{d^*}$, and practically equal to the Redfield ratio for a star identical to our Sun. At distance d_{Star} from the host star, values of $\rho_{N/P}(d_{Star}/d^*)$ higher or lower than 16 would correspond, respectively, to P-limited or N-limited growth conditions (Loladze & Elser 2011). Besides, recent experimental measurements of variability in the cellular stoichiometry of diverse classes of marine eukaryotic phytoplankton under sufficient nutrient conditions reveal a distribution of N:P with an average N:P = 16.2 and a standard deviation of 5 in living cells (Garcia et al. 2018). Therefore, as a conservative ansatz, I propose that values of $\rho_{N/P}(d_{Star}/d^*)$ in the interval [11, 22] can be expected favorable to the emergence on an exoplanet of life as we know it.

In this section, I provide first a criterion to determine d^* for any star system, allowing us to screen confirmed exoplanets with respect to their distance to the cusp point for chemical differentiation. Next, for the subclass of stars liable to host fertile exoplanets, considering the reported distance of an exoplanet to its star d_{Star}, the criterion $\rho_{N/P}(d_{Star}/d^*) \in [11, 22]$ computed thanks to the rescaled Equations (4) and (5), namely, Equation (A12) if $d_{Star} < d^*$ or (A13) if $d_{Star} \geqslant d^*$, will test its potential fertility. Screening the online NASA exoplanet archive (NASA Exoplanet Archive 2023) according to this

procedure provides a probability of occurrence of such Earth analogs and sorts out promising targets.

Generalizing the validity of Equation (2) to any star system, the critical distance d^* is the solution of Equation (6):

$$T_G(R_{PS}) = T_{CB}\left(\frac{d^*}{R_{PS}}\right)^3, \quad (6)$$

where R_{PS} is the protostar radius, in the same unit of length as for d^*, and $T_G(R_{PS})$ is the gas temperature at the protostar surface. Assuming by analogy with our solar system $R_{PS} \cong 1.5R_{star}$, where R_{star} is now the actual stellar radius, as documented in the exoplanet archive, we can estimate $T_G(R_{PS})$ as:

$$T_G(R_{PS}) = T_G(R_{Proto\ Sun})\left(\frac{T_{Stellar\ Surface}}{T_{Sun\ Surface}}\right). \quad (7)$$

The database (NASA Exoplanet Archive 2023) contained 34111 rows at the downloading date, corresponding to 5322 distinct confirmed exoplanets. A subset of 2633 distinct exoplanets allowed to calculate d^* in this way, including 1867 for which T_{Pl}^{eq}, the estimated equilibrium temperature of the exoplanet, was also reported. For calculating T_{Pl}^{eq}, it appears that research groups may use different Bond albedos A_B. Adopting uniformly the classical formula:

$$T_{Pl\_rec}^{eq} = T_{star}\sqrt{\frac{R_{star}}{2d_{star}}}(1 - A_B)^{\frac{1}{4}}, \quad (8)$$

with $A_B = 0.3$ and $T_{star} = T_{Stellar\ Surface}$, allows us to complete to 2633 the subset of available exoplanets equilibrium temperatures, while $T_{Pl\_rec}^{eq}$ remains linearly correlated to the reported T_{Pl}^{eq} ($R^2 = 0.988$). then, another linear correlation ($R^2 = 0.947$) appears in Figure 2 between $Log_{10}(d_{Star}/d^*)$ and $Log_{10}T_{Pl\_rec}^{eq}$. For the solar system, the same plot shows a perfect regression line ($R^2 = 1$). Actually, this broad dependence is expected as the critical distance d^* depends also on R_{star} and T_{star} according to Equations (6) and (7). As both d^* and $T_{Pl\_rec}^{eq}$ are mathematical constructions on the basis of the same data set, the following exact expression holds:

$$\left(\frac{d_{star}}{d^*}\right) = \frac{(1 - A_B)^{\frac{1}{2}}}{2(1.5.T_G(R_{Proto\ Sun})\,/\,(T_{CB}T_{Sun\ Surface}))^{\frac{1}{3}}}\left(\frac{T_{Pl\_rec}^{eq}}{T_{star}^{\frac{5}{6}}}\right)^{-2} = B\left(\frac{T_{Pl\_rec}^{eq}}{T_{star}^{\frac{5}{6}}}\right)^{-2}, \quad (9)$$

with $A_B = 0.3$, $T_G(R_{Proto\ Sun}) = 8.11\ 10^6$ K as reported in (Toulhoat 2022), $T_{CB} = 2.75$ K, and $T_{Sun\ Surface} = 6000$ K, one obtains $B = 3.5343\ 10^{-2}\ K^{\frac{1}{3}}$. This is exactly verified, for exoplanets as well as planets of our solar system. Therefore, the spread as well as outliers in Figure 2 come entirely from the variations in T_{star} (average $\langle T_{star}\rangle = 5393$ K and standard deviation $\sigma(T_{star}) = 1483$ K for the NASA exoplanets archive subset considered).

Equation (9) implies:

$$T_{Pl\_rec}^{eq}(d_{star} = d^*) = T_{Pl\_rec}^{eq*} = B^{1/2}T_{star}^{5/6}. \quad (10)$$

Equation (10) implies $T_{Pl\_rec}^{eq*}(\langle T_{star}\rangle) = 242.1$ K, $T_{Pl\_rec}^{eq*}(\langle T_{star}\rangle + \sigma(T_{star})) = 296.4$ K and $T_{eq\_pl\_rec}^{*}(\langle T_{star}\rangle - \sigma(T_{star})) = 185.2$ K Figure 2 confirms that our solar system is not singular in the known universe. It shows moreover that current exoplanet detection techniques are relatively blind to planets very distant from their stars and therefore cold, i.e., analogs of Jupiter and farther planets in the solar system. A number of Earth analogs might remain undetected as well. As shown in Figure A1 in the Appendix, the distribution of the random variable $Log_{10}(d_{Star}/d^*)$ is well fitted by a log-normal distribution peaking in the vicinity of -1, indicative also that most exoplanets discovered so far are located well within d^*.

The correlation in Figure 2 also shows that the vicinity of the crossing point $Log_{10}(d_{Star}/d^*) = 0$ may support the concept of the habitable Zone (HZ), within which $T_{Pl\_rec}^{eq}$ is compatible with the presence of water in the liquid state at the surface of the exoplanet, provided it is augmented by an atmosphere providing a suitable greenhouse effect.

With ϵ_{HZ} a small real number, in Equation (11) provides thus a first screen of exoplanets within their host star HZ:

$$\left|\ Log_{10}\left(\frac{d_{Star}}{d^*}\right)\ \right| < \epsilon_{HZ}. \quad (11)$$

Indeed, equilibrium temperatures within the habitable zone defined by this criterion obey:

$$T_{pl\_rec}^{eq\_min}(\varepsilon_{HZ}) \leqslant T_{pl\_rec}^{eq\_HZ}\left(\frac{d_{star}}{d^*}\right) \leqslant T_{pl\_rec}^{eq\_max}(\varepsilon_{HZ}), \quad (12)$$

with $T_{pl\_rec}^{eq\_HZ}\left(\frac{d_{star}}{d^*}\right)$ obeying Equation (9) and:

$$T_{pl\_rec}^{eq\_min}(\varepsilon_{HZ}) = 10^{-\varepsilon_{HZ}}T_{Pl\_rec}^{eq*}, \quad (13)$$

$$T_{pl\_rec}^{eq\_max}(\varepsilon_{HZ}) = 10^{\varepsilon_{HZ}}T_{Pl\_rec}^{eq*}. \quad (14)$$

Therefore, for $\varepsilon_{HZ} = 0.2$, $T_{pl\_rec}^{eq\_min}(\langle T_{star}\rangle) = 152.7$ K and $T_{pl\_rec}^{eq\_max}(\langle T_{star}\rangle) = 383.7$ K . It may be concluded that the range of equilibrium temperatures within the habitable zone so defined remains moderate, and on average compatible with that of the Earth ($T_{Pl\_rec}^{eq*} = 264.8$ K in the absence of any greenhouse effect).

Next, taking into account the preceding arguments, fertile exoplanets within HZ will be found verifying (11) and $\rho_{N/P}(d_{Star}/d^*) \in [11, 22]$.

Equations (4) to (11) will make use of astronomical parameters stellar effective temperature st_teff, stellar radius st_rad, planet orbit semi-major axis pl_orbsmax, and planet equilibrium temperature pl_eqt, as reported with a given experimental uncertainty (NASA Exoplanet Archive 2023). It is therefore necessary to estimate error margins on the predicted quantities d^* and $\rho_{N/P}(d_{Star}/d^*)$. The mathematical analysis resulting in these estimates is reported in the Appendix, Section A.2. Screening the database on this basis is possible as long as st_teff, st_rad, and pl-orbsmax are simultaneously reported for a given row. The database subset matching this criterion retains 3178 rows including eventually competing observations of the same exoplanets.

Among these 3178 rows, 214 matched in Equation (11) with $\epsilon_{HZ} = 0.2$, thus corresponding to planets within the HZ. The second criterion $\rho_{N/P}(d_{Star}/d^*) \in [11, 22]$ was matched by 65 rows over 214, corresponding to 49 distinct potentially fertile exoplanets. Observations of the latter among competing ones were selected on the basis of the minimal uncertainty obtained for the prediction of $\rho_{N/P}(d_{Star}/d^*)$.

Tables A1 and A2 in the Appendix list these 49 exoplanets proposed as Earth analogs. Interestingly, the average value of predicted N:P ratios is 17.2 and the rms deviation is 2.9, very close to the average Redfield ratio on Earth: this is obviously a consequence of the random character of the first selection

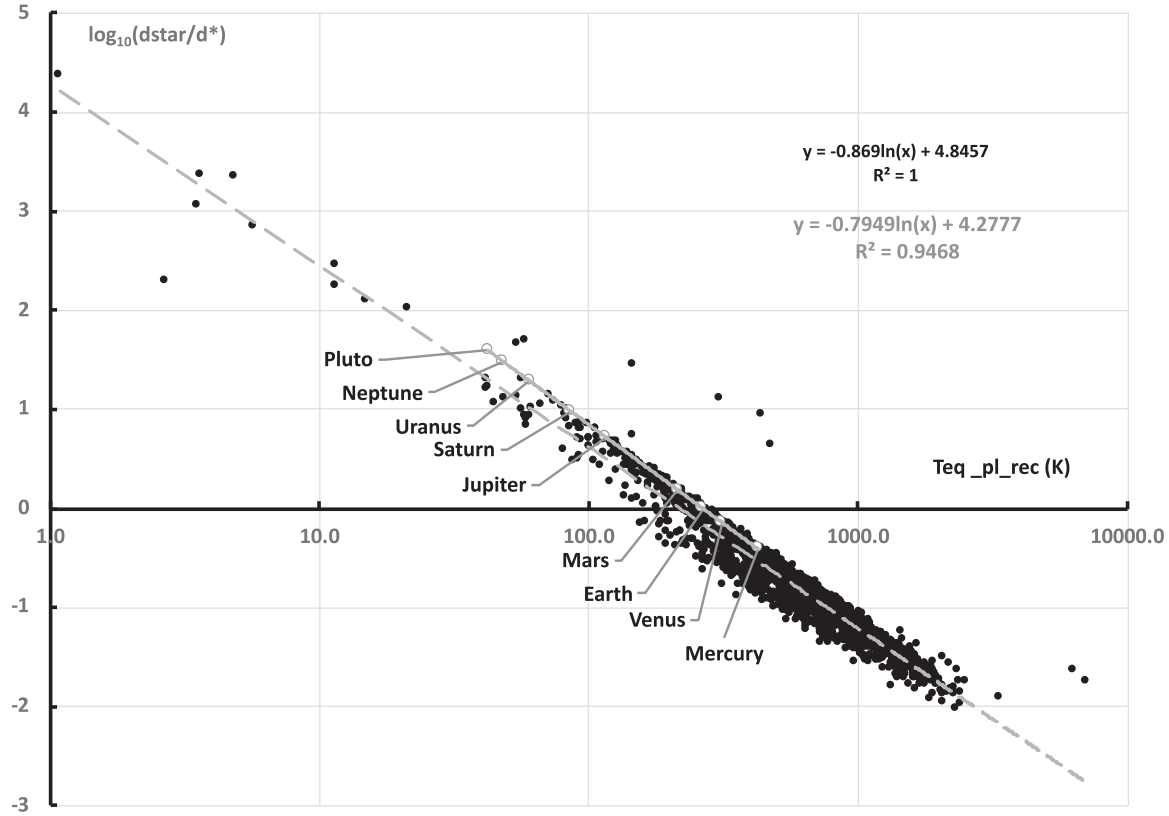

Figure 2. Plots of $\mathrm{Log}_{10}\left(\frac{d_{\mathrm{Star}}}{d^*}\right)$ vs. $\mathrm{Log}_{10}T^{\mathrm{eq}}_{\mathrm{Pl\_rec}}$. Filled black circles, 2633 distinct exoplanets with definable $\frac{d_{\mathrm{Star}}}{d^*}$ and $T^{\mathrm{eq}}_{\mathrm{Pl\_rec}}$; open gray circles, planets in the solar system; regression lines: gray broken line for exoplanets and gray line for the solar system (in inset: equations and squared coefficients of correlation, in gray and black, respectively). Crossing points of regression lines with horizontal axis are 217.3 K for exoplanets and 264.0 K for the solar system (very close to Earth's equilibrium temperature according to Equation (8)).

variable $\mathrm{Log}_{10}(d_{\mathrm{Star}}/d^*)$ sampling the interval [11, 22] through the function $\rho_{\mathrm{N/P}}(d_{\mathrm{Star}}/d^*)$. Besides this sample, the proportion of fertile habitable exoplanets in the database according to these criteria is 2.4%, as obtained through the numerical approach detailed in the Appendix, in Section A.3. This fraction produces already a significant number if extrapolated to the estimate of stars number in the Milky Way only. Improved detection techniques might increase this fraction in the future. This estimate should be also compared to 7.6%, the fraction of confirmed exoplanets within the HZ with $\epsilon_{\mathrm{HZ}} = 0.2$ obtained by integration of the fitted log-normal distribution represented in Figure A1: it may be concluded that on average merely around 30% of exoplanets within the habitable zone as defined here are potentially fertile.

In Figures A2, A3, and A4 of the Appendix are plotted, respectively, for the 49 exoplanets listed in Tables A1 and A2, $\rho_{\mathrm{N/P}}(d_{\mathrm{Star}}/d^*)$ versus the host star distance from the Earth, $\mathrm{Log}_{10}(d_{\mathrm{Star}}/d^*)$ versus the host star distance from the Earth, and $\rho_{\mathrm{N/P}}(d_{\mathrm{Star}}/d^*)$ versus $\mathrm{Log}_{10}(d_{\mathrm{Star}}/d^*)$. Figures A2 and A3 show that the most fertile habitable planets identified reside between 10 and 100 pc from the Earth, so within the Orion arm of our Galaxy. Figure A4 indicates that values of $\rho_{\mathrm{N/P}}(d_{\mathrm{Star}}/d^*)$ are rather well distributed within the HZ.

As mentioned in Tables A1 and A2, average absolute and relative uncertainties are 0.07 for $\mathrm{Log}_{10}(d_{\mathrm{Star}}/d^*)$ and 24% for $\rho_{\mathrm{N/P}}(d_{\mathrm{Star}}/d^*)$. The corresponding error bars are indicated in Figures A2 to A4. Figure A4 in particular reveals that some exoplanets listed in Tables A1 and A2 might actually orbit outside the range assumed habitable, and/or exhibit $\rho_{\mathrm{N/P}}(d_{\mathrm{Star}}/d^*)$ outside the interval of fertility [11, 22]. Conversely, some exoplanets might have escaped this too stringent screen combining habitability and fertility: they might be identified however by extending the screening intervals to $|\mathrm{Log}_{10}(d_{\mathrm{Star}}/d^*)| < 0.28$ and $\rho_{\mathrm{N/P}}(d_{\mathrm{Star}}/d^*) \in [8.4, 27.3]$, i.e., augmenting the initial ranges slightly above the average uncertainties. This procedure resulted in a complementary list of 25 exoplanets reported in Table A3. The average uncertainties on the screening variables were almost unchanged following this extension of ranges. The numerical estimate of the proportion of fertile habitable exoplanets now increases to 4.5%. However, as this numerical estimation is based on the actual distributions of stellar host radii and surface temperatures reported in the exoplanets database, it should be updated in time, as more exoplanets will be confirmed and included in the database, and as detection techniques will improve.

As presented in Tables A4 and A5, most exoplanets found as potentially fertile within the HZ have best masses well above that of the Earth. Only 4 surface gravities over those of 49 exoplanets may be deduced when planet mass and radius are reported together, ranging from 0.41 to 417 Earth surface gravities (g). The corresponding densities range from 0.37 to 498 $\mathrm{g.cm}^{-3}$ (Earth average density 5.513 $\mathrm{g.cm}^{-3}$). It is clear that the knowledge of these properties would allow us to further refine the initial screen by ranges of equilibrium temperature followed by ranges of N:P ratio, in order to identify real analogs of our planet Earth. Unicellular life might in principle accommodate a very large range of surface gravity, but probably not evolve toward large multicellular organisms above some threshold. The existence of

liquid seawater should not be compatible with average planet densities below 1 g.cm^{-3}. In the subset of 4 habitable and potentially fertile exoplanets documented enough, only Kepler-1661 b (1.13 g and 1.62 g.cm^{-3}) and Kepler-22 b (6.36 g and 14.72 g.cm^{-3}) meet these complementary criteria.

5. Corrections for Host Star Metallicities

So far, I incorrectly assumed that protostellar nebulae have very similar chemical compositions although they are enriched in elements beyond H and He as the universe is aging. Stellar metallicity ratios [M/H], or mostly [Fe/H], are indeed reported in the NASA Exoplanets archive so that it is possible to examine the influence of corrections on the photophysical model predictions. The Hypatia catalog has compiled so far relative abundance data for nearly 10,000 stars within 1000 pc of the Sun, including a number of known exoplanet hosts (Hinkel et al. 2014). The elemental abundance data may be considered as usually expressed:

$$\left[\frac{\mathrm{X}}{\mathrm{H}}\right]^{*} = \log_{10}\left[\frac{A_{\mathrm{X}}^{*}/A_{\mathrm{H}}^{*}}{A_{\mathrm{X}}^{\mathrm{SS}}/A_{\mathrm{H}}^{\mathrm{SS}}}\right], \tag{15}$$

where A_{X}^{*} is the relative abundance of element X in the star * system, characterized by a metallicity M, and $A_{\mathrm{X}}^{\mathrm{SS}}$ is the relative abundance of reference in the solar system. The metallicity ratio is generally reported as:

$$M = \left[\frac{\mathrm{Fe}}{\mathrm{H}}\right]^{*}. \tag{16}$$

Another usual alternative definition of the metallicity ratio is:

$$\left[\frac{\mathrm{M}}{\mathrm{H}}\right]^{*} = M_{alt} = \log_{10}\left[\frac{\sum_{all\ \mathrm{X}\ beyond\ \mathrm{He}} A_{\mathrm{X}}^{*}/A_{\mathrm{H}}^{*}}{\sum_{all\ \mathrm{X}\ beyond\ \mathrm{He}} A_{\mathrm{X}}^{\mathrm{SS}}/A_{\mathrm{H}}^{\mathrm{SS}}}\right]. \tag{17}$$

The Hypatia catalog shows that in general $\left[\frac{\mathrm{X}}{\mathrm{H}}\right]^{*}$ and $\left[\frac{\mathrm{Fe}}{\mathrm{H}}\right]^{*}$ are more or less correlated for most stars and elements, with a 2D distribution clearly centered at the origin, the latter characterizing the solar system's analogs.

Let us now consider a set of host stars for which $\left[\frac{\mathrm{X}}{\mathrm{H}}\right]^{*} \sim k_{\mathrm{X}} \left[\frac{\mathrm{Fe}}{\mathrm{H}}\right]^{*} = k_{\mathrm{X}} M$ with M spanning some interval. Screening potentially fertile exoplanets contained in habitable zones of these host stars will involve Equations (A12) and (A13) with prefactors now changed from:

$$\frac{\mathrm{X_{SS}}(N)/\mathrm{X_{SS}}(\mathrm{Si})}{\mathrm{X_{SS}}(P)/\mathrm{X_{SS}}(\mathrm{Si})}\frac{M_P}{M_N} \tag{18}$$

to:

$$\frac{\mathrm{X_{SS}}(N)/\mathrm{X_{SS}}(\mathrm{Si})}{\mathrm{X_{SS}}(P)/\mathrm{X_{SS}}(\mathrm{Si})}\frac{M_P}{M_N}10^{\left(\left[\frac{\mathrm{N}}{\mathrm{H}}\right]^{*}-\left[\frac{\mathrm{P}}{\mathrm{H}}\right]^{*}\right)}, \tag{19}$$

in the cases when both abundances of N and P relative to H are available for the host star, or, when only $\left[\frac{\mathrm{Fe}}{\mathrm{H}}\right]^{*}$ is available and $\left[\frac{\mathrm{N}}{\mathrm{H}}\right]^{*}$ and $\left[\frac{\mathrm{P}}{\mathrm{H}}\right]^{*}$ have to be guessed assuming a linear correlation $\left[\frac{\mathrm{X}}{\mathrm{H}}\right]^{*} \sim k_{\mathrm{X}} \left[\frac{\mathrm{Fe}}{\mathrm{H}}\right]^{*} = k_{\mathrm{X}} M$:

$$\frac{\mathrm{X_{SS}}(N)/\mathrm{X_{SS}}(\mathrm{Si})}{\mathrm{X_{SS}}(P)/\mathrm{X_{SS}}(\mathrm{Si})}\frac{M_P}{M_N}10^{(k_N-k_P)\alpha\left[\frac{\mathrm{Fe}}{\mathrm{H}}\right]^{*}}, \tag{20}$$

where α is another empirical constant allowing consistency between databases: indeed $\alpha \approx 1.06$ is the average ratio between $\left[\frac{\mathrm{Fe}}{\mathrm{H}}\right]^{*}$ reported in the Hypatia Catalog compared to those reported in the NASA archive for the same host stars. Notice that the relative abundance of Si in the host star $\left[\frac{\mathrm{Si}}{\mathrm{H}}\right]^{*}$ cancels in these expressions, so that this information is not needed for our purpose. Depending on the screening interval chosen (e.g., [11–22]), corrections for metallicities to predicted exoplanets N:P ratios may either include them in or exclude them from, the set of potentially fertile. However, error margins to these corrections will increase the uncertainties on the predictions and must be also evaluated.

According to the NASA archive, the 214 exoplanets found in the habitable zone defined by the criterion $|\mathrm{Log}_{10}(d_{\mathrm{Star}}/d^{*})| \leqslant 0.2$ are associated with stellar metallicities $\left[\frac{\mathrm{Fe}}{\mathrm{H}}\right]^{*}$ spanning the interval [−0.89, 0.44], with an average of 0.104 and a standard deviation of 0.23 (with 170 metallicities reported as $\left[\frac{\mathrm{Fe}}{\mathrm{H}}\right]^{*}$, 39 as $\left[\frac{\mathrm{M}}{\mathrm{H}}\right]^{*}$, and 5 unreported). Equation (20) being the most generally applicable for this set with $k_N = 0.8$ and $k_P = 0.99$ reveals an average correction of −1.5 on N:P (standard deviation 3.6) and an average relative uncertainty of 7% on these corrections. Accordingly, five exoplanets should be excluded from the strict interval [11–22] of predicted N:P (PH2 b, HD 156411 b, GJ 3323 c, Kepler-1638 b, Kepler-442 b) but uncertainties on metallicity corrections cancel this diagnostic for all of them. Conversely, four exoplanets should be re-included in the fertile set: HAT-P-13 c, HD 4203 b, Kepler-424 c, but they already belong to the complementary list of Table A3.

The exact Equation (19) can be used for 3 cases only, HD 92788 b, HD 24040 c, and HD 82943 b, but with corrections to N:P of 1.0, −2.25, and 0.0 from 21.1, 17.4, and 16.2, respectively, these exoplanets remain in the range of potential fertility, as listed in Tables A1 and A2.

Tables A4 and A5 present also host star metallicities and corrections to N:P according to Equation (19) for the lists of potentially fertile and habitable exoplanets given in Tables A1 and A2.

In conclusion for this section, in view of the metallicity data available, corrections to the first screening assuming $\left[\frac{\mathrm{Fe}}{\mathrm{H}}\right]^{*} = \left[\frac{\mathrm{Fe}}{\mathrm{H}}\right]^{\mathrm{SS}} = 0$ for all host stars appear minor and do not change significantly the current list of potentially fertile habitable exoplanets. However, for future studies, it should be applied systematically, using at least Equation (20) and at best Equation (19).

Table 3 lists the subset of five sub-Jovian fertile exoplanets found in HZ with mass documented. $T_{\mathrm{Pl\_rec}}^{\mathrm{eq}}$ spans a 28 K interval around the average 249.8 K, a value close to 264.8 K, the latter corresponding as mentioned above, to the Earth in the absence of the current greenhouse effect.

6. Conclusions

In this report, a theoretical basis is proposed for identifying potentially fertile exoplanets inside the habitable zone of their host star. It consists of a set of simple analytical equations calling astronomical parameters associated with confirmed exoplanets. An analysis of the NASA exoplanet archive allows us to conservatively estimate that at least 2.4% of the latter are at the moment suitable as Earth analogs. Corrections for host stars metallicities, when available, do not change significantly the list obtained assuming solar relative abundances of elements. However, such

Table 3
Sub-Jovian Fertile Exoplanets Located in the Habitable Zone($\epsilon_{HZ} = 0.2$) of their Host Stars

Planet Name	Host Star Distance (pc)	$\mathrm{Log}_{10}\left(\frac{d_{\mathrm{Star}}}{d^*}\right)$	$\rho^{corr}_{\mathrm{N/P}}(d_{\mathrm{Star}}/d^*)$	$T^{\mathrm{eq}}_{\mathrm{Pl\_rec}}$	Planet Mass	Density	Gravity	$\left[\frac{\mathrm{Fe}}{\mathrm{H}}\right]$
55 Cnc f	12.6	−0.065	15.6	252	47.8	…	…	0.35
Kepler-1661 b	410.6	−0.056	18.0	247	17.0	1.62	1.14	−0.12
Kepler-22 b	194.6	−0.051	21.5	262	36.0	14.72	6.36	−0.29
HD 191939 g	53.6	−0.047	18.8	254	13.5	…	…	−0.15
HD 40307 g	12.9	−0.044	16.9	234	7.1	…	…	−0.32

Note. d^*(au): critical distance from the host star; d_{Star} (au): distance of the exoplanet from the host star; $\rho^{corr}_{\frac{N}{P}}\left(\frac{d_{\mathrm{Star}}}{d^*}\right)$: predicted nitrogen over phosphorus atomic ratio, corrected for the host star metallicity according to Equation (20); fertility criterion taken as $\rho_{\frac{N}{P}}\left(\frac{d_{\mathrm{Star}}}{d^*}\right) \in [11, 22]$; HZ defined by $-0.20 < \mathrm{Log}_{10}\left(\frac{d_{\mathrm{Star}}}{d^*}\right) \leqslant 0.20$; $T^{\mathrm{eq}}_{\mathrm{Pl\_rec}}$: planet equilibrium temperature according to Equation (8); Planet mass: best plant mass in units of the Earth mass; density in g cm^{-3}; gravity in g (Earth's gravity); $\left[\frac{\mathrm{Fe}}{\mathrm{H}}\right]$: host star metallicity; See Tables A1 to A5 for the Complete Lists.

corrections should be applied as far as possible in order to confirm the screening. Moreover, reasonable ranges of exoplanet average densities and surface gravities should also restrain the screen.

In the future, improved space probing techniques might be focused as a priority in the directions of these potentially fertile exoplanets, in order to detect any signal compatible with life.

The criterion $\rho_{\mathrm{N/P}}(d_{\mathrm{Star}}/d^*) \in [11, 22]$ for this first screening might be somewhat extended to include forms of life adapted to more N- or P-depleted conditions.

Besides, future robotic and manned missions to Mars (predicted $\rho_{\mathrm{N/P}} = 68.5$) might allow us to verify experimentally the predictions that its soil in equilibrium with water and exposed to sunlight, either cannot support the development of phytoplankton species or will select species with N:P much higher than the Redfield ratio.

Acknowledgments

Viacheslav Zgonnik is acknowledged for providing a book (Bertrand & Legendre 2021), which triggered the starting idea for the present work. Louis Legendre is acknowledged for indicating an important reference (Garcia et al. 2018). I am grateful to Pierpaolo Zuddas, Philippe Bertrand, Louis Legendre, and Catherine Jeandel for useful discussions of my drafts. This research has made use of the NASA Exoplanet Archive, which is operated by the California Institute of Technology, under contract with the National Aeronautics and Space Administration under the Exoplanet Exploration Program.

Appendix

A.1. Characterization of the Cusp Point of $\rho_{A/B}(\mathrm{d})$ at $\mathrm{d} = 1$ au

At the cusp point $d = 1$ au, one gets:

$$\rho_{\mathrm{A/B}}(1) = P_{\mathrm{AB}} \exp\left[\frac{\delta_{\mathrm{AB}}\mathrm{IP}}{k_B T_{\mathrm{CB}}} \pi R^2_{\mathrm{PS}}\right], \tag{A1}$$

with notations $P_{\mathrm{AB}} = \frac{\mathrm{X_{SS}}(A)\,/\,\mathrm{X_{SS}(Si)}}{\mathrm{X_{SS}}(B)\,/\,\mathrm{X_{SS}(Si)}} \frac{M_B}{M_A}$ and $\delta_{\mathrm{AB}}\mathrm{IP} = \mathrm{IP(B)} - \mathrm{IP(A)}$.

The left derivative is:

$$\frac{\partial \rho_{\mathrm{A/B}}}{\partial d}^{-}(1) = \frac{\delta_{\mathrm{AB}}\mathrm{IP}}{k_B T_{\mathrm{CB}}} \pi R^2_{\mathrm{PS}} \rho_{\mathrm{A/B}}(1), \tag{A2}$$

and the right derivative is:

$$\frac{\partial \rho_{\mathrm{A/B}}}{\partial d}^{+}(1) = \frac{-2\delta_{\mathrm{AB}}\mathrm{IP}}{k_B T_{\mathrm{CB}}} \pi R^2_{\mathrm{PS}} \rho_{\mathrm{A/B}}(1). \tag{A3}$$

Therefore the cusp point is a minimum for $\delta_{\mathrm{AB}}\mathrm{IP} < 0$ and a maximum for $\delta_{\mathrm{AB}}\mathrm{IP} > 0$.

A.2. Evaluation of Error Margins

In the NASA archive (NASA Exoplanet Archive 2023) exoplanet properties may be displayed on several rows, corresponding to various publication references (column "pl_refname") as several research groups may have contributed to confirm a previous first discovery. Hence, the repeatability of properties for a given exoplanet may provide a first evaluation of error margins on the derived quantities, as calculated from Equations (4) to (11) in the main text.

Besides, for each row (each published observation) properties are bracketed according to uncertainties associated with the method of measurement employed. Error margins associated with derived quantities should then be calculated from the standard methods of calculus of errors, resulting in the following formulae for relative errors assuming uncorrelated errors on the primary measurements:

$$\frac{\Delta d^*}{d^*} = \sqrt{\frac{1}{3}\left(\frac{\Delta T_{\mathrm{star}}}{T_{\mathrm{star}}}\right)^2 + \left(\frac{\Delta R_{\mathrm{star}}}{R_{\mathrm{star}}}\right)^2}. \tag{A4}$$

In order to simplify notations, $\rho^- = \rho_{\mathrm{N/P}}(d_{\mathrm{Star}}/d^*)$ for $d_{\mathrm{Star}} < d^*$, and $\rho^+ = \rho_{\mathrm{N/P}}(d_{\mathrm{Star}}/d^*)$ for $d_{\mathrm{Star}} \geqslant d^*$, and:

$$\frac{\Delta \rho^-}{\rho^-} = \left| \frac{(-\mathrm{IP(A)} + \mathrm{IP(B)})}{k_B T_{\mathrm{CB}}} \pi \left(\frac{R_{\mathrm{PS}}}{d^*}\right)^2 \left(\frac{d_{\mathrm{Star}}}{d^*}\right) \right| \times \sqrt{2\left(\frac{\Delta R_{\mathrm{star}}}{R_{\mathrm{star}}}\right)^2 + 3\left(\frac{\Delta d^*}{d^*}\right)^2 + \left(\frac{\Delta d_{\mathrm{Star}}}{d_{\mathrm{Star}}}\right)^2}, \tag{A5}$$

$$\frac{\Delta \rho^+}{\rho^+} = 2 \left| \frac{(-\mathrm{IP(A)} + \mathrm{IP(B)})}{k_B T_{\mathrm{CB}}} \pi \left(\frac{R_{\mathrm{PS}}}{d_{\mathrm{Star}}}\right)^2 \right| \times \sqrt{\left(\frac{\Delta R_{\mathrm{star}}}{R_{\mathrm{star}}}\right)^2 + \left(\frac{\Delta d_{\mathrm{Star}}}{d_{\mathrm{Star}}}\right)^2}, \tag{A6}$$

where T_{star}, R_{star}, and d_{Star} are the effective temperature and radius of the host star and the distance from the exoplanet to the host star, respectively, and according to column notations in the database:

$$\frac{\Delta T_{\mathrm{star}}}{T_{\mathrm{star}}} = \frac{(st_{tefferr1} - st_{tefferr2})}{2(st\_teff)}, \tag{A7}$$

$$\frac{\Delta R_{\mathrm{star}}}{R_{\mathrm{star}}} = \frac{(st_{raderr1} - st_{raderr2})}{2(st\_rad)}, \tag{A8}$$

$$\frac{\Delta d_{\rm star}}{d_{\rm star}} = \frac{(pl\_orbsmaxerr1 - pl\_orbsmaxerr1)}{2(pl\_orbsmax)}, \quad \text{(A9)}$$

with:

#	COLUMN st_teff:	Stellar Effective Temperature [K]
#	COLUMN st_tefferr1:	Stellar Effective Temperature Upper Uncertainty [K]
#	COLUMN st_tefferr2:	Stellar Effective Temperature Lower Uncertainty [K]
#	COLUMN st_tefflim:	Stellar Effective Temperature Limit Flag
#	COLUMN st_rad:	Stellar Radius [Solar Radius]
#	COLUMN st_raderr1:	Stellar Radius Upper Uncertainty [Solar Radius]
#	COLUMN st_raderr2:	Stellar Radius Lower Uncertainty [Solar Radius]
#	COLUMN pl_orbsmax:	Orbit Semi-major Axis [au])
#	COLUMN pl_orbsmaxerr1:	Orbit Semi-major Axis Upper Uncertainty [au]
#	COLUMN pl_orbsmaxerr2:	Orbit Semi-major Axis Lower Uncertainty [au]

Furthermore:

$$\Delta \mathrm{Log}_{10}\left(\frac{d_{\rm star}}{d^*}\right) = \sqrt{\left(\frac{\Delta d_{\rm star}}{d_{\rm star}}\right)^2 + \left(\frac{\Delta d^*}{d^*}\right)^2}. \quad \text{(A10)}$$

Finally:

$$\frac{\Delta T_{\rm Pl}^{\rm eq}}{T_{\rm Pl}^{\rm eq}} = \frac{(pl\_eqterr1 - pl\_eqterr2)}{2(pl\_eqt)}, \quad \text{(A11)}$$

and:

#	COLUMN pl_eqt:	Equilibrium Temperature [K]
#	COLUMN pl_eqterr1:	Equilibrium Temperature Upper Uncertainty [K]
#	COLUMN pl_eqterr2:	Equilibrium Temperature Lower Uncertainty [K]

When several independent characterizations of the same exoplanet are reported in distinct rows of the NASA exoplanet archive, it is legitimate to retain the one affected by the lower uncertainties, thus producing the lower relative errors from Equations (A4) to (A6).

Tables A1 and A2 present the results of these estimations of error margins for the potentially habitable and fertile exoplanets identified according to the procedure detailed in the main text. Averages of the latter were used to indicate error margins in Figures A2 to A4.

A.3. Numerical Evaluation of the Fraction of Fertile Exoplanets within the Habitable Zone

Let us express ρ^- and ρ^+ according to Equations (4) and (5) of the main text, transposed from the solar system to any stellar system by rescaling the unit of length:

$$\rho^-\left(\frac{R_{PST}}{d^*}, \frac{d_{\rm star}}{d^*}\right) = \frac{\mathrm{X_{SS}(A)}/\mathrm{X_{SS}(Si)}}{\mathrm{X_{SS}(B)}/\mathrm{X_{SS}(Si)}}\frac{M_B}{M_A} \times \exp\left[\frac{(-\mathrm{IP(A)} + \mathrm{IP(B)})}{k_B T_{\rm CB}}\pi\left(\frac{R_{PST}}{d^*}\right)^2\left(\frac{d_{\rm star}}{d^*}\right)\right], \quad \text{(A12)}$$

and:

$$\rho^+\left(\frac{R_{PST}}{d^*}, \frac{d_{\rm star}}{d^*}\right) = \frac{\mathrm{X_{SS}(A)}/\mathrm{X_{SS}(Si)}}{\mathrm{X_{SS}(B)}/\mathrm{X_{SS}(Si)}}\frac{M_B}{M_A} \times \exp\left[\frac{(-\mathrm{IP(A)} + \mathrm{IP(B)})}{k_B T_{\rm CB}}\pi\left(\frac{R_{PST}}{d^*}\frac{d^*}{d_{\rm star}}\right)^2\right]. \quad \text{(A13)}$$

Besides, according to Equations (6) and (7) of the main text:

$$\frac{R_{PST}}{d^*} = \left(\frac{T_G(R_{\rm Protosun})}{T_{\rm CB}}\frac{T_{\rm Star}}{T_{\rm Sun}}\right)^{\frac{-1}{3}}. \quad \text{(A14)}$$

Therefore, both ratios are basically functions of two random variables $\frac{d_{\rm star}}{d^*}$ and $T_{\rm Star}$.

Figure A5 demonstrates that these variables are uncorrelated ($R^2 = 0.0263$). Figure A6 presents the distribution of $\frac{R_{PST}}{d^*}$ encompassing 4647 distinct exoplanets for which $T_{\rm Star}$ has been reported. This distribution may be characterized as a skewed normal law spanning the interval [0.0037 au, 0.015 au] peaked at 0.007165 au, slightly above $R_{\rm Protosun}$ (dashed vertical line). It shows that 92% of exoplanet-hosting stars so far detected are warmer than our Sun, and the current sampling of cooler host stars underestimates their occurrence.

Application of Equation (A12) or (A13) at $\frac{d_{\rm star}}{d^*} = 1$ predicts the atomic ratio N/P at the cusp point so that the lower limit of $\frac{R_{PST}}{d^*}$ corresponding to the upper limit of the screening interval for this ratio can be determined. For the interval [11, 22] it is 0.0065446 au, and over 99% of host stars of exoplanets detected so far have $\frac{R_{PST}}{d^*}$ above this limit and therefore may host fertile exoplanets in their habitable zone.

In order to evaluate the probability of an exoplanet being potentially fertile within the habitable zone, let us consider two bidimensional grids with nodes spaced at regular intervals along variables $\frac{R_{PST}}{d^*} > 0.0065446$ au and $\mathrm{Log}_{10}(d_{\rm Star}/d^*) \in [-\epsilon_{\rm HZ},\ 0]$ for the first one and $\mathrm{Log}_{10}(d_{\rm Star}/d^*) \in [\ 0,\ \epsilon_{\rm HZ}\ ]$ for the second. Let us calculate ρ^- at nodes of the first grid and ρ^+ at nodes of the second one from Equations (A12) and (A13), respectively. A logical test returning 1 if the value for an "active" node belongs to the chosen screening interval (e.g., [11, 22]) and 0 if the value is outside, will allow us to count the active nodes in a grid. The ratio of active to total number of nodes is an estimate of the required probability for one grid, expected to converge rapidly as the number of nodes in the grids is increased. The average over both grids holds for the probability $P_1(\epsilon_{\rm HZ})$ over the whole HZ. These grids cover practically all realizations of $\frac{R_{PST}}{d^*}$ in the database, but only the realizations of $\mathrm{Log}_{10}(d_{\rm Star}/d^*)$ in $[-\epsilon_{\rm HZ},\ \epsilon_{\rm HZ}]$. The

Table A1
List of the First 24 of 49 Fertile Exoplanets Found in the Habitable Zone (HZ)

Rowid	Planet Name	Host Star Distance (pc)	$\mathrm{Log}_{10}\left(\frac{d_{\rm Star}}{d^*}\right)$	A.U. 1	$\rho_{\rm N/P}(d_{\rm Star}/d^*)$	R.U. 2 (%)	$T_{\rm Pl}^{\rm eq}$ (K)	R.U. 3 (%)
462	GJ 1002 c	4.8	−0.179	0.082	14.3	0.44	182	0.027
575	GJ 357 d	9.4	−0.145	0.081	15.1	0.27	220	0.027
708	GJ 876 b	4.7	−0.144	0.033	13.4	0.18	…	…

Table A1
(Continued)

Rowid	Planet Name	Host Star Distance (pc)	$\mathrm{Log_{10}}\left(\frac{d_{\mathrm{Star}}}{d^*}\right)$	A.U. 1	$\rho_{\mathrm{N/P}}(d_{\mathrm{Star}}/d^*)$	R.U. 2 (%)	$T_{\mathrm{Pl}}^{\mathrm{eq}}$ (K)	R.U. 3 (%)
24214	Kepler-443 b	802.3	−0.123	0.267	21.8	0.64	⋯	⋯
24212	Kepler-442 b	366.0	−0.122	0.331	19.4	0.82	⋯	⋯
20540	Kepler-296 f	⋯	−0.107	0.178	12.3	0.69	⋯	⋯
8828	Kepler-1229 b	265.5	−0.101	0.087	11.8	0.52	212	0.085
3350	HIP 56640 b	122.3	−0.088	0.030	18.3	0.09	⋯	⋯
12833	Kepler-1544 b	335.1	−0.086	0.051	18.4	0.24	269	0.084
20975	Kepler-309 c	544.6	−0.084	0.160	12.3	0.93	202	⋯
2816	HD 38801 b	91.4	−0.081	0.149	21.0	0.75	⋯	⋯
2860	HD 4203 b	81.4	−0.075	0.040	21.9	0.19	⋯	⋯
13359	Kepler-1593 b	638.2	−0.074	0.052	16.7	0.25	260	0.083
32050	PH2 b	343.9	−0.073	0.054	21.9	0.26	281	0.025
114	55 Cnc f	12.6	−0.065	0.013	18.3	0.06	⋯	⋯
3211	HD 92788 b	34.7	−0.062	0.023	21.2	0.07	⋯	⋯
2014	HD 156411 b	56.9	−0.058	0.046	21.8	0.22	⋯	⋯
14030	Kepler-1661 b	410.6	−0.056	0.021	17.0	0.09	243	⋯
2516	HD 218566 b	28.8	−0.054	0.031	15.9	0.15	⋯	⋯
126	7 CMa b	19.8	−0.051	0.073	14.8	0.30	⋯	⋯
17978	Kepler-22 b	194.6	−0.051	0.031	18.8	0.12	262	⋯
2317	HD 191939 g	53.6	−0.047	0.044	17.5	0.16	278	0.022
2913	HD 48265 b	90.5	−0.046	0.049	19.0	0.17	⋯	⋯
13798	Kepler-1638 b	1525.5	−0.045	0.168	20.3	0.84	304	0.115

Note. Rowid: row number in the NASA exoplanet archive; $\boldsymbol{d^*}$ (au): critical distance from the host star; $\boldsymbol{d_{\mathrm{Star}}}$ (au): distance of the exoplanet from the host star; $\boldsymbol{\rho_{\mathrm{N/P}}(d_{\mathrm{Star}}/d^*)}$: predicted nitrogen over phosphorus atomic ratio; fertility criterion taken as $\boldsymbol{\rho_{\mathrm{N/P}}\left(\frac{d_{\mathrm{Star}}}{d^*}\right) \in [11, 22]}$; HZ defined by $\boldsymbol{-0.20 < \mathrm{Log_{10}}\left(\frac{d_{\mathrm{Star}}}{d^*}\right) \leqslant 0.20}$; A.U., R.U.: absolute and relative uncertainties, respectively, in %, affecting the previous column (see Section A.2 of this appendix for their estimations).

Table A2
List of the 25 Last of 49 Fertile Exoplanets Found in the Habitable Zone (HZ)

Rowid	Planet Name	Host Star Distance (pc)	$\mathrm{Log_{10}}\left(\frac{d_{\mathrm{Star}}}{d^*}\right)$	A.U. 1	$\rho_{\mathrm{N/P}}(d_{\mathrm{Star}}/d^*)$	R.U. 2 (%)	$T_{\mathrm{Pl}}^{\mathrm{eq}}$ (K)	R.U. 3 (%)
2843	HD 40307 g	12.9	−0.044	0.086	14.6	0.47	255	⋯
2905	HD 4732 c	54.8	−0.043	0.091	14.9	0.46	⋯	⋯
2881	HD 44219 b	52.9	−0.039	0.057	18.9	0.29	⋯	⋯
5194	KIC 3526061 b	401.2	−0.026	0.056	12.8	0.27	⋯	⋯
23880	Kepler-419 c	1011.4	−0.026	0.048	20.9	0.22	⋯	⋯
2876	HD 43197 b	62.4	−0.024	0.021	16.1	0.08	⋯	⋯
2627	HD 24040 c	46.6	−0.024	0.031	17.4	0.13	⋯	⋯
24423	Kepler-452 b	551.7	−0.020	0.114	16.9	0.62	265	0.053
158	BD+14 4559 b	49.4	−0.013	0.083	11.9	0.36	⋯	⋯
24424	Kepler-453 b	442.8	−0.010	0.018	14.8	0.09	⋯	⋯
1983	HD 153950 b	48.5	−0.003	0.039	17.0	0.19	⋯	⋯
3143	HD 82943 b	27.6	−0.003	0.034	16.0	0.16	⋯	⋯
2036	HD 159868 b	55.9	−0.002	0.159	14.1	0.50	⋯	⋯
2670	HD 28185 b	39.4	0.004	0.022	15.2	0.08	⋯	⋯
1644	HD 108874 b	59.5	0.005	0.029	15.2	0.13	⋯	⋯
1535	HD 100777 b	49.5	0.007	0.035	15.2	0.15	⋯	⋯
1905	HD 142415 b	35.5	0.009	0.028	17.7	0.13	⋯	⋯
2893	HD 45364 c	34.4	0.019	0.0197	17.2	0.11	⋯	⋯
24581	Kepler-47 c	1025.0	0.022	0.031	18.8	0.15	⋯	⋯
1855	HD 137388 b	40.5	0.026	0.026	17.0	0.10	⋯	⋯
2256	HD 188015 b	50.7	0.030	0.036	20.5	0.19	⋯	⋯
2451	HD 210277 b	21.3	0.035	0.020	21.0	0.08	⋯	⋯
1809	HD 128356 b	26.2	0.040	0.046	18.0	0.22	⋯	⋯
727	GJ 876 e	4.7	0.081	0.045	14.8	0.38	⋯	⋯
552	GJ 3323 c	5.4	0.115	0.256	20.7	1.85	⋯	⋯
Averages		⋯	⋯	**0.07**	**17.2**	**0.24**	**248.7**	**0.06**

Note. Rowid: row number in the NASA exoplanet archive; $\boldsymbol{d^*}$(au): critical distance from the host star; $\boldsymbol{d_{\mathrm{Star}}}$ (au): distance of the exoplanet from the host star ; $\boldsymbol{\rho_{\mathrm{N/P}}\left(\frac{d_{\mathrm{Star}}}{d^*}\right)}$: predicted nitrogen over phosphorus atomic ratio; fertility criterion taken as $\boldsymbol{\rho_{\mathrm{N/P}}\left(\frac{d_{\mathrm{Star}}}{d^*}\right) \in [11, 22]}$; HZ defined by $\boldsymbol{-0.20 < \mathrm{Log_{10}}\left(\frac{d_{\mathrm{Star}}}{d^*}\right) \leqslant 0.20}$; A.U., R.U.: absolute and relative uncertainties, respectively, in %, affecting the previous column (see Section A.2 of this appendix for their estimations).

probability $P_2(\epsilon_{HZ})$ of the latter may be accurately estimated as the integral of the log-normal distribution shown in Figure A1 between $-\epsilon_{HZ}$ and ϵ_{HZ}. It follows that the probability for an exoplanet to be both fertile and in the habitable zone is $P(\epsilon_{HZ}) = P_1(\epsilon_{HZ})P_2(\epsilon_{HZ})$.

Probabilities $P(\epsilon_{HZ})$ estimated following this numerical procedure provided in the main text for $\epsilon_{HZ} = 0.2$ and $\epsilon_{HZ} = 0.28$, respectively, 0.024 and 0.045, were obtained for grids 40 lines x 28 columns and 57 lines x 28 columns, respectively. The whole procedure was easily implemented in an Excel worksheet.

A.4. Supplementary Tables

Table A3
Complementary List of 25 Fertile Exoplanets

Rowid	Planet Name	Host Star Distance (pc)	$\mathrm{Log_{10}}\left(\frac{d_{Star}}{d^*}\right)$	A.U. 1	$\rho_{N/P}(d_{Star}/d^*)$	R.U. 2 (%)	T_{Pl}^{eq} (K)	R.U. 3 (%)
474	GJ 1148 b	11.0	−0.2578	0.033	26.2	0.08	…	…
32431	TOI-2257 b	57.8	−0.2495	0.049	26.0	0.11	256	0.152
31514	LHS 1140 b	15.0	−0.2431	0.079	21.9	0.20	230	0.087
549	GJ 3293 d	20.2	−0.2354	0.080	24.6	0.23	…	…
4352	K2-288 B b	65.6	−0.2060	0.219	19.9	0.54	226	0.097
1930	HD 147379 b	10.8	−0.1967	0.109	25.7	0.32	…	…
26798	Kepler-62 e	300.9	−0.1477	0.037	26.3	0.10	270	0.056
2490	HD 216520 c	19.6	−0.1352	0.024	26.0	0.06	…	…
1921	HD 145934 b	227.9	−0.1348	0.053	24.0	0.12	…	…
13961	Kepler-1653 b	…	−0.1346	0.046	23.8	0.12	284	0.081
3028	HD 69830 d	12.6	−0.1256	0.032	27.1	0.07	…	…
829	HAT-P-13 c	246.8	−0.1102	0.061	26.6	0.16	340	0.026
2891	HD 45364 b	34.4	−0.1043	0.020	24.7	0.05	…	…
23961	Kepler-424 c	698.6	−0.0966	0.124	23.7	0.30	…	…
2857	HD 4203 b	81.4	−0.0965	0.031	24.7	0.07	…	…
2078	HD 164509 b	53.1	−0.0819	0.032	24.8	0.09	…	…
5599	KOI-351 h	848.3	−0.0773	0.145	25.1	0.35	…	…
2189	HD 180617 b	5.9	−0.0698	0.028	9.3	0.10	…	…
43	30 Ari B b	44.7	−0.0628	0.032	24.6	0.09	…	…
16213	Kepler-186 f	177.6	−0.0546	0.175	9.6	0.63	…	…
2042	HD 1605 c	88.8	−0.0001	0.110	10.4	0.46	…	…
3142	HD 82943 b	27.6	0.0475	0.024	27.0	0.08	…	…
2765	HD 34445 f	46.1	0.0520	0.061	27.0	0.25	…	…
1692	HD 113538 b	16.3	0.0737	0.165	24.5	0.79	…	…
5689	Kapteyn c	3.9	0.1058	0.137	22.5	0.80	…	…

Note. Rowid: row number in NASA exoplanet archive; $\boldsymbol{d^*}$(au): critical distance from the host star; $\boldsymbol{d_{Star}}$ (au): distance of the exoplanet from the host star; $\boldsymbol{\rho_{N/P}\left(\frac{d_{Star}}{d^*}\right)}$: predicted nitrogen over phosphorus atomic ratio; fertility criterion taken as $\boldsymbol{\rho_{N/P}\left(\frac{d_{Star}}{d^*}\right) \in [8.4, 27.3]}$; HZ defined by $\boldsymbol{-0.28 < \mathrm{Log_{10}}\left(\frac{d_{Star}}{d^*}\right) \leqslant 0.28}$; A.U., R.U.: absolute and relative uncertainties, respectively, in %, affecting the previous column (see Section A.2 of this appendix for their estimations).

Table A4
List of the First 24 of 49 Fertile Exoplanets Found in the Habitable Zone (HZ)

Planet Name	$\mathrm{Log_{10}}\left(\frac{d_{Star}}{d^*}\right)$	$\left[\frac{Fe}{H}\right]$	$\rho_{N/P}^{corr}(d_{Star}/d^*)$	Δ	Planet Mass	Dens	Gravity	$T_{Pl\_rec}^{eq}$
GJ 1002 c	−0.179	−0.25	16.1	1.8	1.4	…	…	183.8
GJ 357 d	−0.145	−0.12	15.9	0.9	6.1	…	…	199.7
GJ 876 b	−0.144	0.21	12.1	−1.3	672.2	…	…	189.5
Kepler-443 b	−0.123	−0.01	21.9	0.1	…	…	…	249.6
Kepler-442 b	−0.122	−0.37	23.1	3.6	…	…	…	235.3
Kepler-296 f	−0.107	−0.12	13.0	0.7	…	…	…	194.3
Kepler-1229 b	−0.101	0.16	11.0	−0.8	…	…	…	193.1
HIP 56640 b	−0.088	−0.03	18.6	0.3	1166.4	…	…	241.9
Kepler-1544 b	−0.086	−0.08	19.1	0.7	…	…	…	243.4
Kepler-309 c	−0.084	−0.28	14.0	1.7	…	…	…	202.7
HD 38801 b	−0.081	0.25	18.7	−2.3	3082.3	…	…	263.4
HD 4203 b	−0.075	0.40	18.2	−3.7	708.8	…	…	272.0
Kepler-1593 b	−0.074	−0.10	17.5	0.8	…	…	…	237.1
PH2 b	−0.073	−0.08	22.7	0.8	…	…	…	273.0

Table A4
(Continued)

Planet Name	$\mathrm{Log_{10}}\left(\frac{d_{\mathrm{Star}}}{d^*}\right)$	$\left[\frac{\mathrm{Fe}}{\mathrm{H}}\right]$	$\rho^{corr}_{\mathrm{N/P}}(d_{\mathrm{Star}}/d^*)$	Δ	Planet Mass	Dens	Gravity	$T^{\mathrm{eq}}_{Pl\_\mathrm{rec}}$
55 Cnc f	−0.065	0.35	15.6	−2.7	47.8	⋯	⋯	252.0
HD 92788 b	−0.062	0.30	18.5	−2.7	1179.1	⋯	⋯	273.7
HD 156411 b	−0.058	−0.12	23.0	1.2	235.2	⋯	⋯	279.1
Kepler-1661 b	−0.056	−0.12	18.0	1.0	17.0	1.62	1.14	246.6
HD 218566 b	−0.054	0.30	13.9	−2.0	62.9	⋯	⋯	239.7
7 CMa b	−0.051	0.21	13.4	−1.4	826.3	⋯	⋯	232.7
Kepler-22 b	−0.051	−0.29	21.5	2.7	36.0	14.72	6.36	261.6
HD 191939 g	−0.047	−0.15	18.8	1.3	13.5	⋯	⋯	253.9
HD 48265 b	−0.046	0.40	15.8	−3.2	467.2	⋯	⋯	265.3
Kepler-1638 b	−0.045	−0.76	28.9	8.6	⋯	⋯	⋯	275.1

Note. d^*(au): critical distance from the host star; d_{Star} (au): distance of the exoplanet from the host star; $\left[\frac{\mathrm{Fe}}{\mathrm{H}}\right]$: host star metallicity; $\rho^{corr}_{\mathrm{N/P}}(d_{\mathrm{Star}}/d^*)$: predicted nitrogen over phosphorus atomic ratio, corrected for the host star metallicity according to Equation (20); fertility criterion taken as $\rho^{corr}_{\mathrm{N/P}}(d_{\mathrm{Star}}/d^*) \in [11, 22]$; HZ defined by $-0.20 < \mathrm{Log_{10}}(d_{\mathrm{Star}}/d^*) \leqslant 0.20$; Δ: correction for metallicity on atomic ratio N:P; Planet mass: best planet mass in units of the Earth mass; Dens.: density in g.cm^{-3}; Gravity in g (Earth's gravity); $T^{\mathrm{eq}}_{\mathrm{Pl\_rec}}$: planet equilibrium temperature according to Equation (8), in K.

Table A5
List of the Last 25 of 49 Fertile Exoplanets Found in the Habitable Zone (HZ)

Planet Name	$\mathrm{Log_{10}}\left(\frac{d_{\mathrm{Star}}}{d^*}\right)$	$\left[\frac{\mathrm{Fe}}{\mathrm{H}}\right]$	$\rho^{corr}_{\mathrm{N/P}}(d_{\mathrm{Star}}/d^*)$	Δ	Planet Mass	Dens	Gravity	$T^{\mathrm{eq}}_{Pl\_\mathrm{rec}}$
HD 40307 g	−0.044	−0.32	16.9	2.3	7.1	⋯	⋯	233.9
HD 4732 c	−0.043	0.01	14.8	−0.1	753.2	⋯	⋯	237.1
HD 44219 b	−0.039	0.03	18.6	−0.3	184.3	⋯	⋯	267.3
KIC 3526061 b	−0.026	0.12	12.1	−0.7	5768.6	⋯	⋯	227.5
Kepler-419 c	−0.026	0.18	19.3	−1.6	2320.1	⋯	⋯	288.8
HD 43197 b	−0.024	0.40	13.4	−2.7	190.7	⋯	⋯	253.4
HD 24040 c	−0.024	0.20	15.9	−1.5	63.9	⋯	⋯	263.6
Kepler-452 b	−0.020	0.21	15.4	−1.6	⋯	⋯	⋯	261.7
BD+14 4559 b	−0.013	0.17	11.0	−0.9	330.5	⋯	⋯	225.4
Kepler-453 b	−0.010	0.09	14.2	−0.6	16.0	0.37	0.42	249.9
HD 153950 b	−0.003	−0.01	17.1	0.1	937.6	⋯	⋯	270.2
HD 82943 b	−0.003	0.23	14.4	−1.6	489.1	⋯	⋯	262.4
HD 159868 b	−0.002	−0.06	14.5	0.4	540.3	⋯	⋯	247.8
HD 28185 b	0.004	0.23	13.7	−1.5	1875.2	⋯	⋯	251.1
HD 108874 b	0.005	0.26	13.5	−1.7	451.3	⋯	⋯	248.3
HD 100777 b	0.007	0.25	13.6	−1.7	327.4	⋯	⋯	245.3
HD 142415 b	0.009	0.13	16.6	−1.0	530.8	⋯	⋯	259.6
HD 45364 c	0.019	⋯	18.2	1.0	174.5	⋯	⋯	239.6
Kepler-47 c	0.022	−0.25	21.1	2.3	8899.0	497.55	416.92	244.8
HD 137388 b	0.026	0.19	15.6	−1.4	63.6	⋯	⋯	227.3
HD 188015 b	0.030	0.25	18.2	−2.3	462.1	⋯	⋯	243.2
HD 210277 b	0.035	0.22	19.0	−2.0	410.0	⋯	⋯	237.8
HD 128356 b	0.040	0.17	16.7	−1.4	282.9	⋯	⋯	212.6
GJ 876 e	0.081	⋯	14.1	−0.8	18.0	⋯	⋯	145.4
GJ 3323 c	0.115	−0.27	23.5	2.8	2.3	⋯	⋯	135.8

Note. d^*(au): critical distance from the host star; d_{Star} (au): distance of the exoplanet from the host star; $\left[\frac{\mathrm{Fe}}{\mathrm{H}}\right]$: host star metallicity; $\rho^{corr}_{\mathrm{N/P}}(d_{\mathrm{Star}}/d^*)$: predicted nitrogen over phosphorus atomic ratio, corrected for the host star metallicity according to Equation (20); fertility criterion taken as $\rho^{corr}_{\mathrm{N/P}}(d_{\mathrm{Star}}/d^*) \in [11, 22]$; HZ defined by $-0.20 < \mathrm{Log_{10}}(d_{\mathrm{Star}}/d^*) \leqslant 0.20$; Δ: correction for metallicity on atomic ratio N:P; Planet mass: best planet mass in units of the Earth mass; Dens.: density in g.cm^{-3}; Gravity in g (Earth's gravity); $T^{\mathrm{eq}}_{Pl\_\mathrm{rec}}$: planet equilibrium temperature according to Equation (8), in K.

A.5. Supplementary Figures

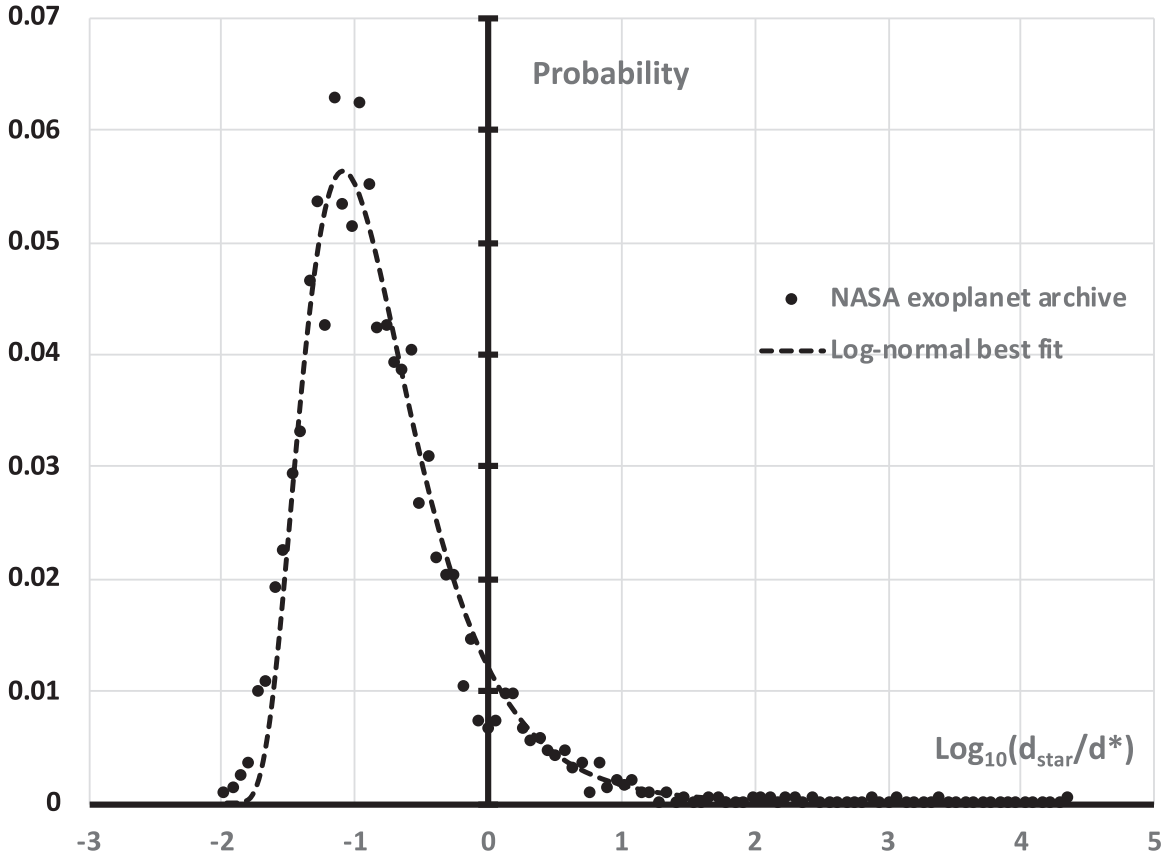

Figure A1. Distribution of the random variable $\mathrm{Log}_{10}\left(\frac{d_{\mathrm{Star}}}{d^*}\right)$ (filled circles) and its best fit by the Log-normal distribution of expected value $\mu = 0.1263$ and standard deviation $\sigma = 0.43984$ (dotted curve). Integration of this log-normal distribution within the interval $\left|\mathrm{Log}_{10}\left(\frac{d_{\mathrm{Star}}}{d^*}\right)\right| < \mathbf{0.2}$ allow us to determine that 7.6% of confirmed exoplanets in the NASA archive are within this interval.

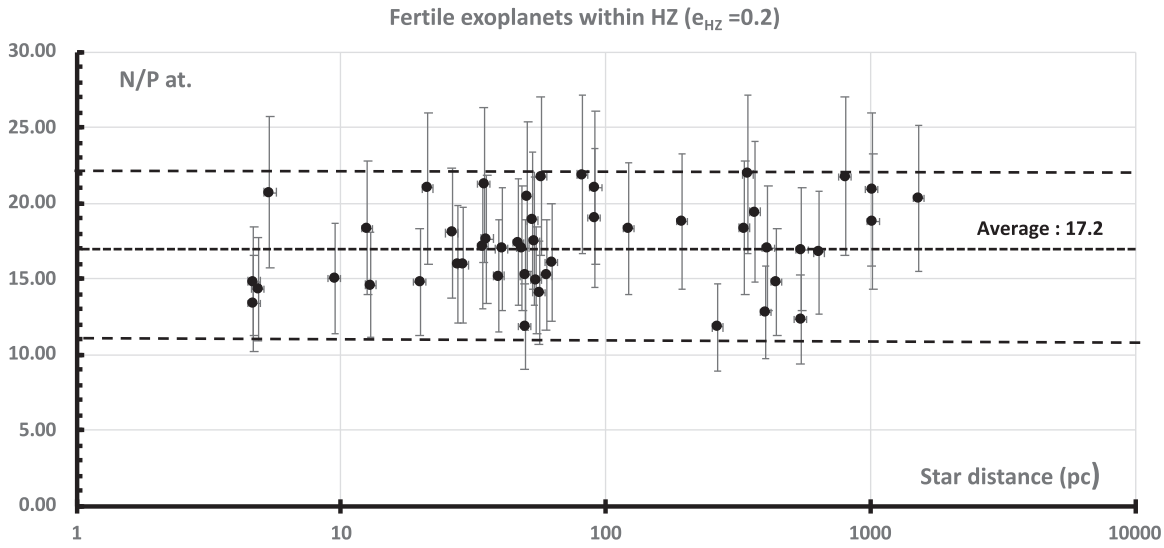

Figure A2. Predicted atomic ratio Nitrogen over Phosphorus as a function of the host star distance from Earth (in parsec) for the 49 exoplanets listed in Tables A1 and A2 (filled circles). This graph shows that detected exoplanets predicted fertile within the Habitable Zone are mostly located inside the Orion arm of our Galaxy. Dotted line: average N/P atomic ratio. Dashed lines limit the range of selection [11–22]. Error bars on N/P correspond to 24%, the calculated average relative uncertainty indicated in Table A2.

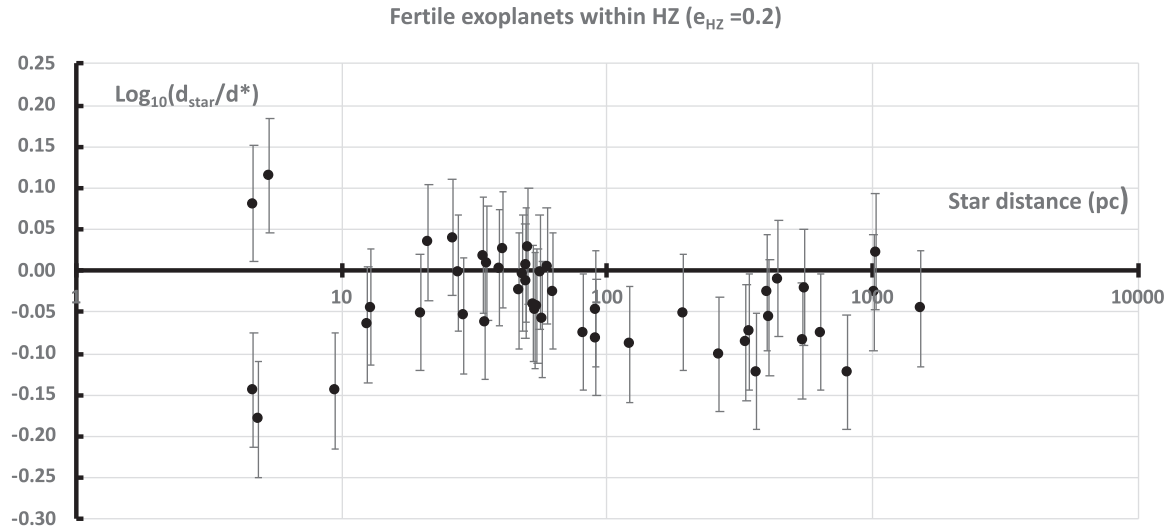

Figure A3. Predicted $\mathrm{Log}_{10}\left(\frac{d_{\mathrm{Star}}}{d^*}\right)$ as a function of the host star distance from Earth (in parsec) for the 49 exoplanets listed in Tables A1 and A2 (filled circles). Vertical error bars correspond to the average uncertainty of 0.07 This graph shows further that detected exoplanets predicted fertile within the Habitable Zone are mostly located inside the Orion arm of our Galaxy.

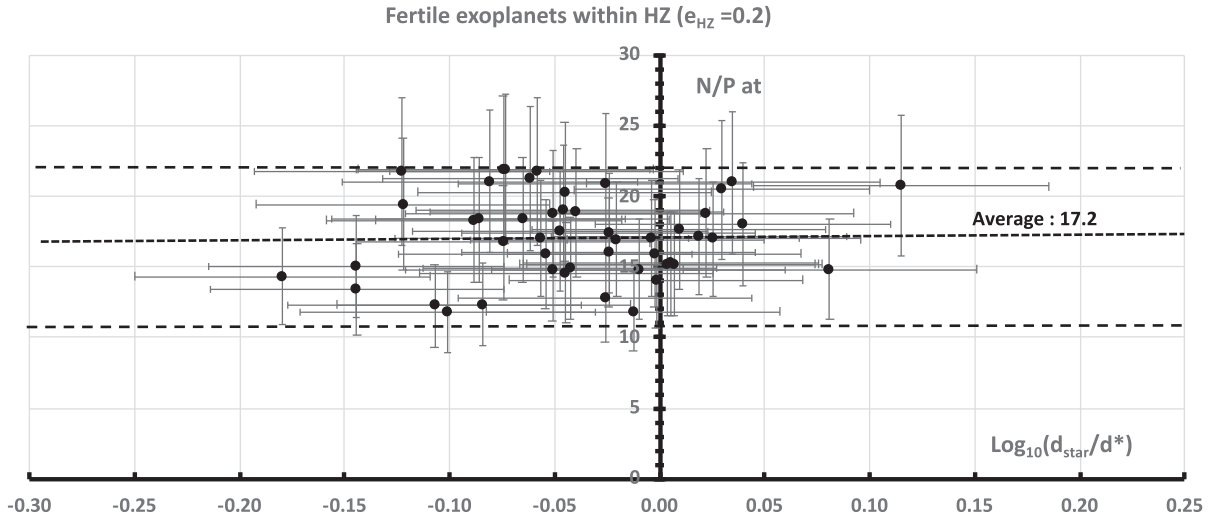

Figure A4. Predicted atomic ratio nitrogen over phosphorus as a function of $\mathrm{Log}_{10}\left(\frac{d_{\mathrm{Star}}}{d^*}\right)$ for the 49 fertile exoplanets listed in Tables A1 and A2 (filled circles). This graph shows that the predicted (N/P) appears randomly valued between 11 and 22, with an average of 17.2, within the Habitable Zone as defined by $\left|\mathrm{Log}_{10}\left(\frac{d_{\mathrm{Star}}}{d^*}\right) < 0.2\right|$. dotted line: average N/P atomic ratio. Dashed lines limit the range of selection [11–22]. Error bars on N/P correspond to 24%, the calculated average relative uncertainty indicated in Table A2. Error bars on $\mathrm{Log}_{10}\left(\frac{d_{\mathrm{Star}}}{d^*}\right)$ correspond to the average absolute error of 0.07 indicated in Table A2.

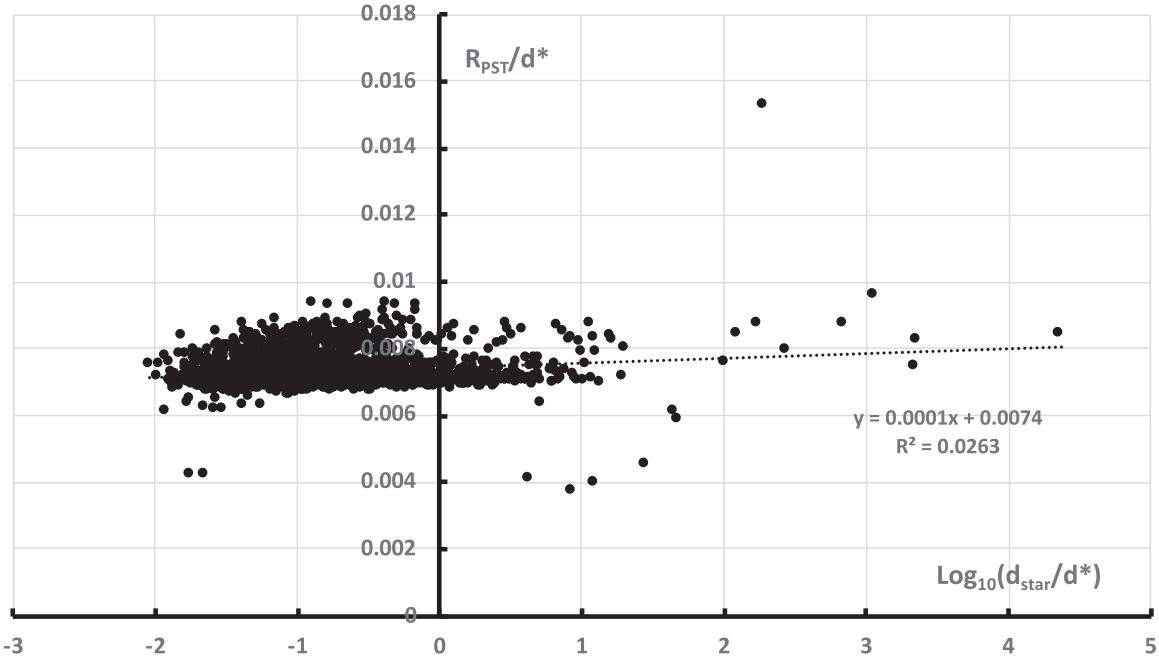

Figure A5. Plot of random variable $\frac{R_{PST}}{d^*}$ against random variable $\mathrm{Log}_{10}\left(\frac{d_{\mathrm{Star}}}{d^*}\right)$ showing the absence of a significant correlation. (Inset equation of regression line and squared coefficient of correlation).

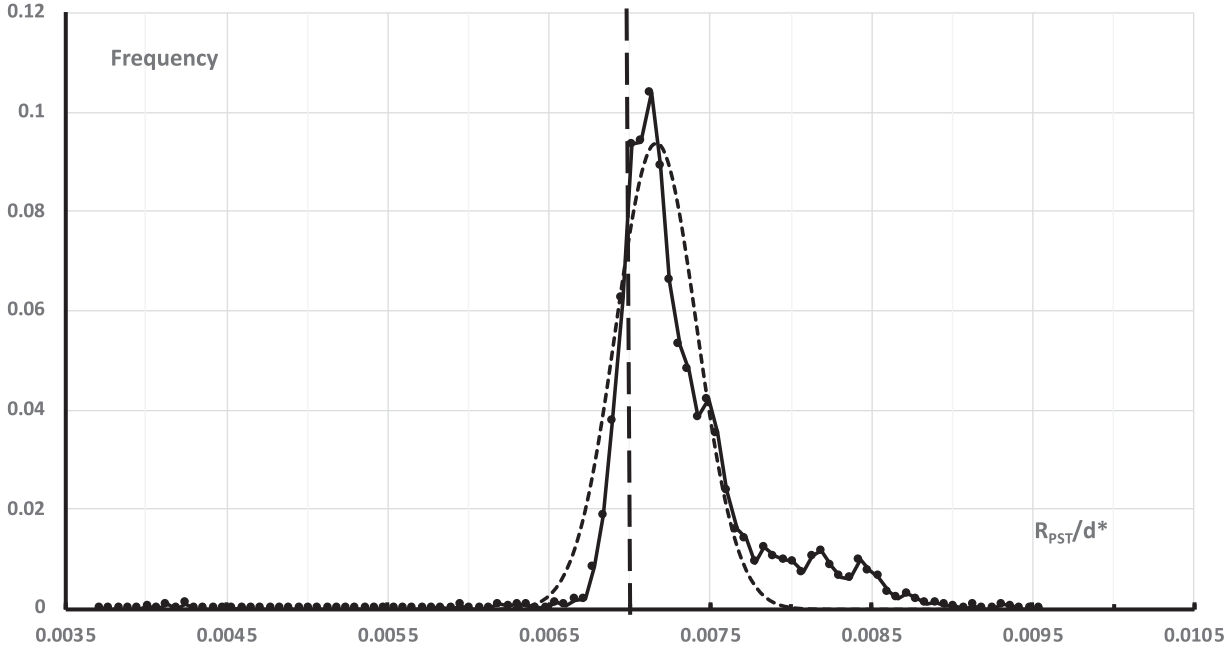

Figure A6. Distribution of the random variable $\frac{R_{PST}}{d^*}$ for the NASA exoplanet archive. The sample involves 4657 distinct exoplanets (some sharing the same host star). The filled circles and the continuous line trace the observed histogram. Dotted curve: best-fit normal law ($\mu = 0.00716467$, $\sigma = 0.00025$). The dashed vertical line locates the Sun.

ORCID iDs

Hervé Toulhoat https://orcid.org/0000-0001-8359-4454

References

Bertrand, P., & Legendre, L. 2021, Earth, Our Living Planet (Berlin: Springer)
Diehl, A., & & Bach, W. 2020, GGG, 21, e2020GC009385
Falkowski, P. G., & & Davis, C. S. 2004, Natur, 431, 131
Garcia, N. S., Sexton, J., Riggins, T., et al. 2018, Front. Microbiol., 9, 543
Hinkel, N. R., Timmes, F. X., Young, P. A, et al. 2014, AJ, 148, 54
Lodders, K. 2003, ApJ, 591, 1220
Loladze, I., & & Elser, J. J. 2011, EcolL, 14, 244
NASA Exoplanet Archive 2023, https://exoplanetarchive.ipac.caltech.edu, downloaded on Monday April 3, 2023, at 01:39:02
Redfield, A. C. 1934, in James Johnstone Memorial Volume, ed. R. J. Daniel (Liverpool: Liverpool Univ. Press), 176
Redfield, A. C. 1936, Natur, 138, 1013
Redfield, A. C. 1958, AmSci, 46, 204
Toulhoat, H., & & Zgonnik, V. 2022, ApJ, 924, 83